J. Fluid Mech. (1982), *vol.* 122, *pp.* 235–250
Printed in Great Britain

Numerically computed multiple steady states of vertical buoyancy-induced flows in cold pure water

By IBRAHIM EL-HENAWY, BRIAN HASSARD, NICHOLAS KAZARINOFF,
Department of Mathematics, SUNY/B, 106 Diefendorf Hall, Buffalo, NY 14214

BENJAMIN GEBHART
MEAM, Towne Building, University of Pennsylvania, Philadelphia, PA 19104

AND JOSEPH MOLLENDORF
Department of Mechanical and Aerospace Engineering,
335 Engineering East (R3), SUNY/B, Amherst, NY 14260

(Received 16 June 1981 and in revised form 3 March 1982)

The laminar, boundary-layer, natural convection flow adjacent to a vertical, heated or cooled, flat surface submerged in quiescent cold water was studied. The results demonstrate for the first time the existence of multiple steady-state solutions in a *natural* convection flow. The calculated velocity profiles, over a range of the parameters, are compared with recent corresponding velocity measurements of Wilson & Vyas (1979) and of Carey & Gebhart (1981). The newly found additional steady-state solutions are of considerable practical interest because the heat-transfer rates for a pair of solutions (with determining physical parameters and boundary conditions otherwise identical) are sometimes vastly different. An important consequence of this study is the possible relationship of multiple steady-state solutions to the recently observed unsteadiness in some such flows.

1. Introduction

The decrease of hydrogen bonding between water molecules causes the density of cold water to first increase with increasing temperature above the equilibrium melting point. The other density-controlling mechanism, thermal molecular motion, opposes this effect. Eventually a density maximum is reached at about 4 °C in pure water at atmospheric pressure. An important consequence is that bodies of water, such as lakes, freeze from the top down. Also, in vertical buoyancy-induced flows in both cold pure and saline water there is the possibility of a bidirectional buoyancy force. This results in the transition from net upflow to net downflow as the ambient temperature T_∞ is varied for a fixed density-maximum temperature T_m.

A discussion of the early investigations of such vertical, natural convection flows is given by Gebhart & Mollendorf (1978). The present investigation uses a density relation for pure and saline water that was developed by Gebhart & Mollendorf (1977). This relation was designed to be a simple but accurate expression for the motion-causing buoyancy force in low-temperature pure and saline water wherein effects of the density maximum are important.

A number of recent theoretical and experimental studies by Bendell & Gebhart (1976), Carey & Gebhart (1981), Carey, Gebhart & Mollendorf (1980), Gebhart, Carey & Mollendorf (1979), Johnson (1979), Mollendorf, Johnson & Gebhart (1981), Wilson & Vyas (1979), and Wilson & Lee (1981) have added considerably to the understanding of these interesting and complex flows. However, several questions remain to challenge both theorists and experimenters. The question addressed in this paper concerns the range of parameter values over which there exist solutions to the governing steady, laminar, boundary-layer approximations to the time-independent Navier–Stokes–energy equations. These new numerical results provide conjectured explanations for the unsteadiness in time, observed recently by Carey & Gebhart (1981) and Wilson & Vyas (1979). The observed unsteadiness arose in the vertical velocity component of the motion of cold pure water adjacent to a vertical ice slab, in the parameter range for which a bidirectional buoyancy force has significant effects.

In the present study, multiple steady-state solutions of the government similarity equations were found over two distinct ranges of the flow parameters. At Prandtl number $Pr = 11{\cdot}6$ we have found multiple steady-state solutions for the density-extremum parameter $R = (T_m - T_\infty)/(T_0 - T_\infty)$ in the following ranges: $R = 0{\cdot}291\,81$–$0{\cdot}454\,02$ and $R = 0{\cdot}151\,49$–$0{\cdot}151\,80$ as located on figure 3. For example, when T_0 is taken to be 0 °C, as for a melting ice surface, and T_m is taken to be 4·029 325 °C, these ranges of R correspond to ambient temperature ranges $T_\infty = 5{\cdot}6896$–$7{\cdot}3800$ °C and $T_\infty = 4{\cdot}7487$–$4{\cdot}7504$ °C (see §3 and figures 3–8). As far as we know, these are the first multiple steady-state solutions found for any natural convection flow, although multiple steady-state solutions have been known in forced flows for over 25 years. They were found for flow past a wedge by Stewartson (1953), and more recently in chemical-reactor problems by Cohen (1973), and in the von Kármán swirling-disk problem by Zandbergen & Dijkstra (1977) and Lentini & Keller (1978, 1980). Stewartson's (1953) multiple steady-state solutions for flow over a wedge have been used in aerodynamics as a basis for calculation of flows past separation (see e.g. Lees & Reeves 1964; Orimi & Reeves 1976). The present work may provide a similar basis for dealing with separated natural convection flows.

Our finding of multiple steady-state solutions is interesting in view of recent experimental studies by Carey & Gebhart (1981) and Wilson & Vyas (1979). The combination of our results and theirs suggests the tentative conjecture that the flow wanders between unstable equilibria (steady states). We call this a 'configurational instability'. A comparison of the numerically computed solutions presented here with the velocity measurements of some flows observed by Wilson & Vyas (1979) seems to indicate that the observed flows are indeed close to one or another computed steady-state solution, as well as being intermediate between them at different times (see §4).

There is another important question: why does there remain a range of values of R, between $0{\cdot}151\,80$ and $0{\cdot}291\,81$, for which we were not able to compute any solutions of the boundary-layer equations? Wilson & Lee (1981) encountered a similar gap in R in which they could not find solutions of the time-independent Navier–Stokes–energy equations. Yet, for parameter values in this gap, experiments indicate that flow still occurs. Could it be that no steady flows exist when the buoyancy force has these stronger bidirectional characteristics? These questions will also be discussed in §4.

We close this section with a brief summary of the main features of the new solutions

we have computed and the method used to find them. These solutions all exhibit reversals in the vertical component of velocity $u \propto f'$ (see figures 6–8, and note that the very weak reversal in figure 6(a) is indiscernable with the scales used). Inside reversals arise for $0{\cdot}291\,81 \leqslant R \leqslant 0{\cdot}454\,02$, and outside reversals are found for $0{\cdot}151\,49 \leqslant R \leqslant 0{\cdot}151\,80$. For example, the solution in figure 8(a), which is initially negative on $(0, 2+)$, shows an inside reversal, and the solutions in figure 7(a), which are negative for $\eta > 3$, show outside reversals. The new solutions have ever more pronounced inside reversals as R increases from $0{\cdot}291\,81$ to $0{\cdot}454\,02$ ($-\phi'(0)$ decreases from $0{\cdot}492\,50$ to $0{\cdot}005\,00$). The relative values of the minimum and maximum values of solutions at the two ends of this range are:

at $R = 0{\cdot}454\,02$ and $-\phi'(0) = 0{\cdot}005\,00$

$$\frac{\max\limits_{[0,\infty)}[-f'(\eta)]}{\max\limits_{[0,\infty)}[f'(\eta)]} \approx \frac{-f'(1{\cdot}08)}{f'(3{\cdot}55)} \approx \frac{0{\cdot}0535}{0{\cdot}1204} \approx 0{\cdot}444;$$

and at $R = 0{\cdot}291\,81$ and $-\phi'(0) = 0{\cdot}492\,50$

$$\frac{\max\limits_{[0,\infty)}[-f'(\eta)]}{\max\limits_{[0,\infty)}[f'(\eta)]} \approx \frac{-f'(0{\cdot}25)}{f'(1{\cdot}80)} \approx \frac{0{\cdot}0095}{0{\cdot}0565} \approx 0{\cdot}17;$$

f', ϕ and η are defined later.

The heat-transfer rate at the vertical flat surface ($y = \eta = 0$), determined for the previously known steady-state solution at $R = 0{\cdot}454\,02$, is $-\phi'(0) = 0{\cdot}975\,20$. That found for the second steady-state solution at the same R is $-\phi'(0) = 0{\cdot}005\,00$. The ratio of these heat-transfer rates is approximately 200. This is striking, and would be easily measurable should the existence of both computed solutions arise in experiments.

The new solutions have been discovered by two means. The first is a simple and well-known tool, that of suspending (adding below) a new differential equation $dR/d\eta = 0$ to the system studied. This additional equation permits one to introduce a new boundary condition containing a parameter that can be varied as desired to generate a family of solutions to the boundary-value problem by continuation. The second means is the use of state-of-the-art two-point boundary-value problem codes, a collocation code COLSYS by Ascher, Christiansen & Russell (1978) and a multiple-shooting code BOUNDS by Bulirsch, Stoer & Deuflhard (1982) (see also Bulirsch & Stoer 1966; Diekhoff *et al.* 1977).

2. The boundary-value problem

The Navier–Stokes–energy equations for two-dimensional natural convection of pure water adjacent to an impermeable, vertical, isothermal surface are (see figure 1)

$$\mathbf{w}_t + (\mathbf{D}\mathbf{w})\,\mathbf{w} = -\frac{1}{\rho}\operatorname{grad} p + g\mathbf{F}(T, T_\infty) + \nu\Delta\mathbf{w}, \tag{2.1a}$$

$$T_t + \mathbf{w}.(\nabla T) = \tilde{\alpha}\Delta T, \tag{2.1b}$$

$$\operatorname{div}\mathbf{w} = 0, \tag{2.1c}$$

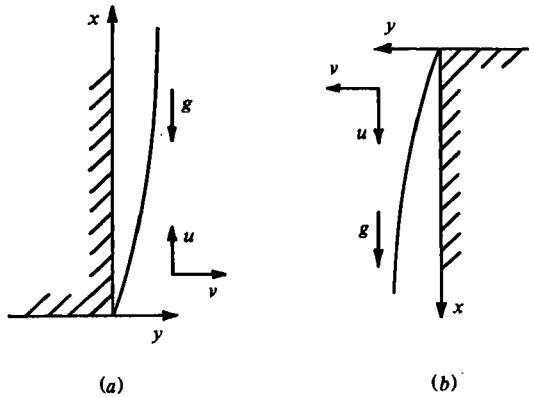

FIGURE 1. The coordinate systems: (*a*) upflow, (*b*) downflow.

where $\mathbf{w} = (uv)^{\mathrm{tr}}$. Here u, v, T and p are respectively the x- and y-components of velocity, the temperature and the motion pressure (the local static pressure minus the local hydrostatic pressure), at location (x, y) at time t. The matrix $(\mathbf{Dw})$ is the Jacobian of w. The constant quantities ρ, g, ν, and $\tilde{\alpha}$ are respectively the fluid density at (x, y, t), the gravitational acceleration, kinematic viscosity, and thermal diffusivity. The term $g\mathbf{F}(T, T_\infty)$ is the buoyancy force. In these equations, terms corresponding to heat generated by friction and pressure stress in the moving fluid, and involving derivatives of ρ, have been neglected.

We study steady-state solutions of (2.1), that is, solutions independent of t. We assume that $T(x, \infty) = T_\infty$ is independent of x, unstratified, and that $\rho = \rho(T)$. Let $\rho_\infty = \rho(T_\infty)$, let ρ_{m} be the maximum density of water, and let T_{m} be defined by $\rho(T_{\mathrm{m}}) = \rho_{\mathrm{m}}$. With T_0 being the surface temperature (e.g. 0 °C as with a melting ice surface), the density-extremum parameter has been previously defined as

$$R = \frac{T_{\mathrm{m}} - T_\infty}{T_0 - T_\infty},$$

and we conventionally call

$$\phi = \frac{T - T_\infty}{T_0 - T_\infty},$$

the temperature-excess ratio. The buoyancy force $g\mathbf{F}(T, T_\infty)$ has been formulated by Gebhart & Mollendorf (1977) as

$$\begin{aligned} g\mathbf{F}(T, T_\infty) &= \begin{pmatrix} \mp g(\rho_\infty - \rho)/\rho_{\mathrm{m}} \\ 0 \end{pmatrix} \\ &= \begin{pmatrix} \mp g\alpha[|\phi - R|^q - |R|^q] \\ 0 \end{pmatrix} |T_0 - T_\infty|^q, \end{aligned} \tag{2.2}$$

where for pure water at 1 bar pressure $q = 1{\cdot}894816$, $\alpha = 9{\cdot}297173 \times 10^{-6}(°\mathrm{C})^{-q}$ and $T_{\mathrm{m}} = 4{\cdot}029325$ °C. These values arise in a density correlation that fits the data to within 3·5 ppm for pure water (Mollendorf & Gebhart 1977). The ' + ' sign is used in (2.2) for flows with the characteristics of figure 1(*a*), which occur for $R \leqslant R_{\mathrm{u}} \approx 0{\cdot}15$, largely upflow, and the ' − ' sign is used for flows as in figure 1(*b*), which occur for $R \geqslant R_{\mathrm{d}} \approx 0{\cdot}3$, largely downflow (see Gebhart & Mollendorf 1978). One configuration of T_0, T_{m}, and T_∞ that yields $R < 0$ is illustrated in figure 2. The corresponding flow

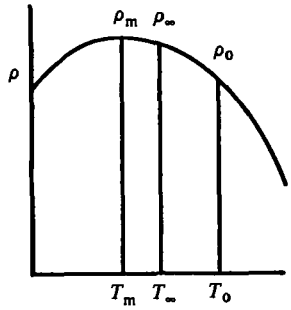

FIGURE 2. Water density ρ as a function of temperature T. Also shown are conditions of T_0 and T_∞ for which $R < 0$.

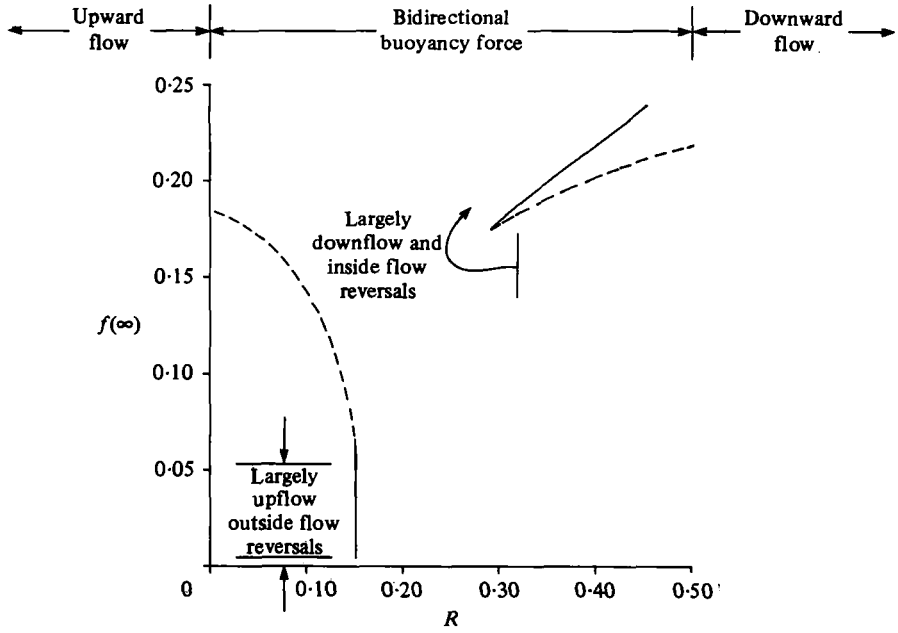

FIGURE 3. Mass flow rate $f(\infty)$ and regions of flow, buoyancy-force reversal, and multiple solutions. The lower R-region is largely upflow, the upper one largely downflow. Dashed curves correspond to the solutions of Carey *et al.* (1980), the solid ones correspond to the present results. No solutions exist for $f(\infty) < 0$.

is upward everywhere, and the ' + ' sign is used in (2.2) to obtain the buoyancy force in (2.1).

Following Gebhart & Mollendorf (1978) and Carey *et al.* (1980), we introduce a stream function ψ and make a similarity transformation of the time-independent forms of (2.1*a–c*):

$$\psi(x,y) \equiv \nu G f(\eta), \quad \eta = yG/4x,$$

where

$$G = 4(\tfrac{1}{4}Gr_x)^{\frac{1}{4}}, \quad Gr_x = \frac{gx^3}{\nu^2}\alpha|T_0 - T_\infty|^q.$$

The new independent variable is η, and the new dependent variables are f, ϕ, P, where

$$u = \psi_y = \nu G^2 f'(\eta)/4x,$$
$$v = -\psi_x = -\nu G(3f - \eta f')/4x,$$
$$p = \rho \nu^2 G^2 P/(4x)^2.$$

In the new variables (2.1*a–c*) become, after we divide the equations by $\nu^2 G^4/(4x)^3$,

$$2(f')^2 - 3ff'' = \frac{2P + \eta P'}{G^2} + f''' \mp [|\phi - R|^q - |R|^q] + \frac{-4f' + \eta f'' + \eta^2 f'''}{G^2}, \tag{2.3a}$$

$$\frac{1}{G}[9ff' - \eta(f')^2 - 3\eta ff''] = \frac{1}{G}\left[-P' + \eta f''' - f'' + \frac{-15f - 9\eta f' + 6\eta^2 f'' + \eta^3 f'''}{G^2}\right], \tag{2.3b}$$

$$-3Prf\phi' = \phi'' + \frac{\eta^2 \phi'' + 5\eta\phi'}{G^2}, \tag{2.3c}$$

where Pr is $\nu/\tilde{\alpha}$ and we have cancelled a common factor of $4x(T_0 - T_\infty)\tilde{\alpha}/\nu^2 G^4$ in (2.3*c*). Here $\alpha \approx 9{\cdot}3 \times 10^{-6}(°\mathrm{C})^{-q}$, terrestrial $g \approx 9{\cdot}81\ \mathrm{m/s^2}$ and $\nu \approx 1{\cdot}67 \times 10^{-6}\ \mathrm{m^2/s}$,

$$G^2 = \frac{8(g\alpha)^{\frac{1}{2}}}{\nu} |T_0 - T_\infty|^q x^{\frac{3}{2}}$$
$$\approx 46000\, |T_0 - T_\infty|^q x^{\frac{3}{2}};$$

this is large if, say, $x \geqslant 0{\cdot}02\mathrm{m}$ and $T_0 - T_\infty = 5\ °\mathrm{C}$. Thus we may neglect the G^{-2} terms in (2.3) compared with the first terms on the right-hand sides. Then, after multiplying (2.3*b*) by G we obtain the familiar similarity boundary-layer equations:

$$f''' = \pm [|\phi - R|^q - |R|^q] + 2(f')^2 - 3ff'', \tag{2.4a}$$

$$P' = 3\eta(f')^2 - 9ff' - f'' \pm \eta[|\phi - R|^q - |R|^q], \tag{2.4b}$$

$$\phi'' = -3Prf\phi'. \tag{2.4c}$$

Equation (2.4*b*) yields $P'(\eta)$ after (2.4*a*) and (2.4*c*) are solved subject to the boundary conditions (2.5) below, and then P' can be integrated to obtain the motion pressure p.

We are now ready to impose the boundary conditions implied by a quiescent and unstratified ambient medium and an impermeable, isothermal, vertical surface lying at $y = 0$ and $x \geqslant 0$. These are

$$u(x,0) = v(x,0) = u(x,\infty) = T(x,0) - T_0 = T(x,\infty) - T_\infty = 0$$

or

$$f(0) = f'(0) = f'(\infty) = 1 - \phi(0) = \phi(\infty) = 0. \tag{2.5}$$

The equations (2.4*a*, *c*) together with the boundary conditions (2.5) form a two-point boundary-value problem for (f, ϕ) on the η-interval $[0, \infty)$. Gebhart & Mollendorf (1978) and Carey *et al.* (1980) treated (2.4*a*, *c*) and (2.5) numerically. They used simple shooting to integrate the equations as an initial-boundary-value problem on intervals $[0, \eta_\infty]$. The boundary conditions were applied at $\eta = 0$. The boundary conditions at ∞ were applied at η_∞ and were supplemented by the known asymptotic behaviour of (f, ϕ) at $\eta = \infty$.

3. Numerical methods and results

We have solved the boundary-value-problem (2.4*a*, *c*)–(2.5) using two different codes: COLSYS (Ascher *et al.* 1978) and BOUNDS (Bulirsch *et al.* 1982). COLSYS is an adaptive orthogonal collocation code. It was chosen because one may fix the degree of the polynomials employed in the spline approximation so as to avoid potential difficulties caused by lack of smoothness (discontinuous second derivative) in the expression for the buoyancy force. BOUNDS is a multiple-shooting code, employing the Bulirsch–Stoer rational extrapolation algorithm (Bulirsch & Stoer 1966) for solutions of initial-value problems. It was chosen to confirm the results obtained using COLSYS because it provides highly accurate results. The discontinuity in $f^{(\mathrm{iv})}$ at the point where $\phi(\eta) = R$ does not apparently have an adverse effect upon solution of the boundary-value problem using BOUNDS. Roughly the same amount of computational effort was required when using either COLSYS or BOUNDS; that was about 10 CP s per solution on a CDC Cyber 174 (compilation of the driving programs under FTN4.8, OPT = 2).

To generate the families of solutions, three different continuation schemes were used. Simple continuation in the parameter R was used to recompute and continue the families of solutions found previously by Carey *et al.* (1980). When difficulty with this scheme was encountered, shortly beyond the points where the simple shooting method of Carey *et al.* diverged, continuation in either $f'(\infty)$ (R near 0·1517) or $\phi'(0)$ (R near 0·292) was employed. To implement continuation with respect to $f(\infty)$ or $\phi'(0)$, R was taken as an additional unknown in (2.4). That is, the equation $R' = 0$ was appended to the system, along with an additional boundary condition specifying either $f(\infty)$ or $\phi'(0)$, and then the new system was solved for a sequence of values of $f(\infty)$ or $\phi'(0)$ to obtain families of solutions.

The boundary-value problems were solved on intervals $[0, \eta_\infty]$, with $\eta_\infty = 60$, 80, 100, ..., 500, and the solutions compared. When the solutions corresponding to successive lengths agreed with each other to five significant figures, the interval was accepted as sufficiently large. Near the limit points ('noses') that are present in figure 4(*a*) for $R \approx 0{\cdot}151\,80$, $f(\infty) \approx 0{\cdot}045\,00$ and $R \approx 0{\cdot}151\,49$, $f(\infty) \approx 0{\cdot}015\,00$ it was necessary to solve on intervals up to length 500 before the above criterion was met. Near the limit point in figure 5 at $R \approx 0{\cdot}291\,81$, $f(\infty) \approx 0{\cdot}175\,11$, $-\phi'(0) \approx 0{\cdot}492\,50$ an interval length of 300 sufficed.

The main features of the new solutions of (2.4)–(2.5) we have found as compared to the previously known solutions are illustrated in figures 6–8. The values of $f(\infty)$, $-\phi'(0)$, $f''(0)$, and R and η_∞ associated with the families of solutions we have computed are given in tables 1 and 2. All of these were computed using COLSYS. The solutions illustrated in figures 6–8 were independently computed and verified to five-digit accuracy using BOUNDS. All of our new solutions exhibit reversals in the x-component of velocity u (which is proportional to f' for fixed x). As R was increased from 0·15 we found that $f'(5{\cdot}03)$ first became negative at a value of R between 0·151 70 and 0·151 62. The computed velocity profile at $R = 0{\cdot}151\,72$ and $Pr = 11{\cdot}6$ reversed from positive to negative at $\eta = 5{\cdot}025 \pm 0{\cdot}005$. Carey *et al.* (1980) found this η-value to be 'approximately 5·5'.

As R was decreased from 0·33 we found that $f'(0{\cdot}01)$ first became negative at a value of R between 0·324 29 and 0·324 14. The computed velocity profile at

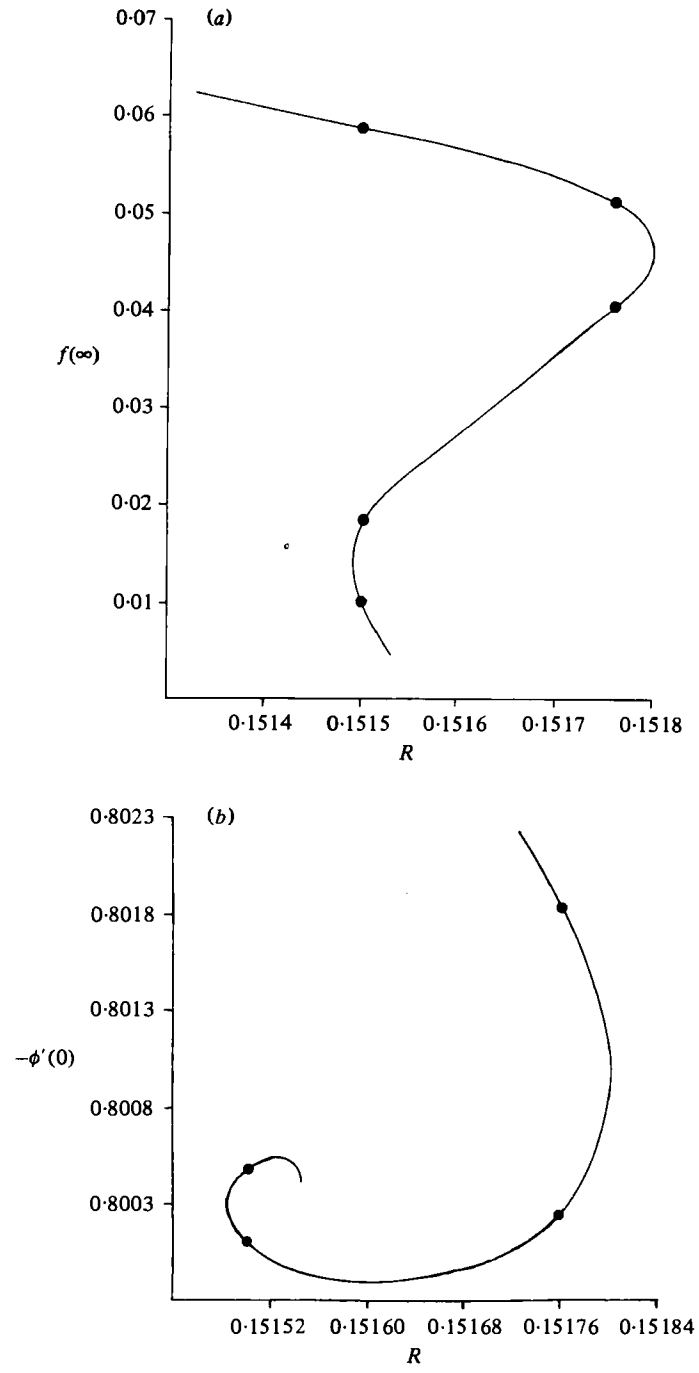

FIGURE 4. Details of the variation of (*a*) mass-flow rate $f(\infty)$ and (*b*) heat-transfer rate $-\phi'(0)$ with R in the region of largely upflow. The large solid dots correspond to solutions illustrated in figures 6 and 7.

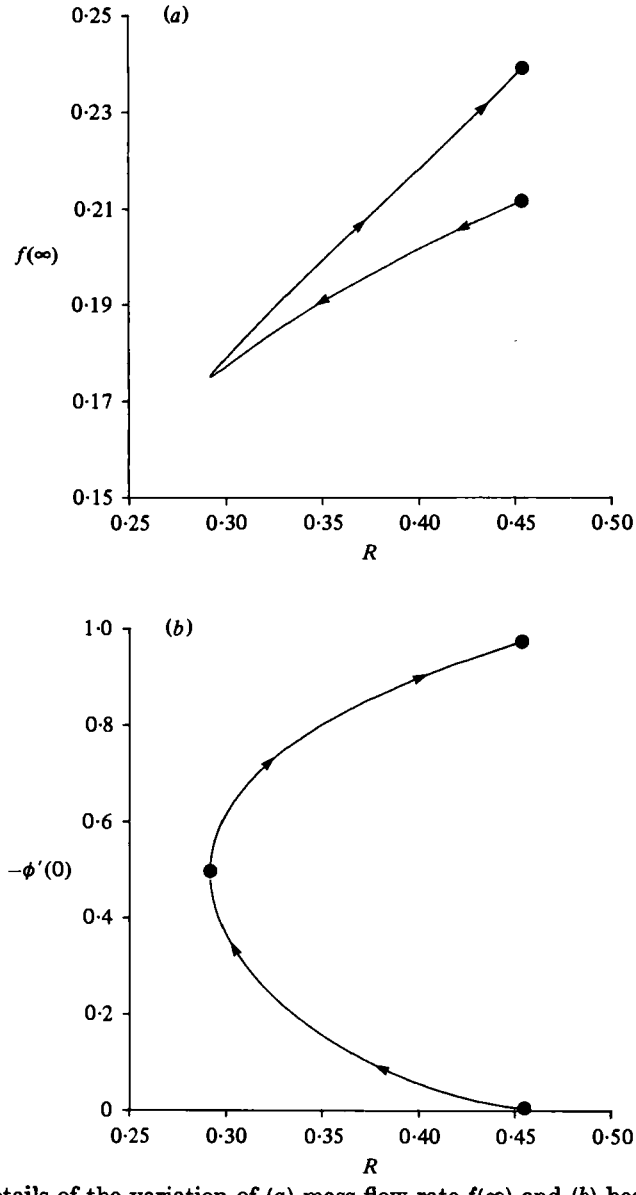

FIGURE 5. Details of the variation of (*a*) mass-flow rate $f(\infty)$ and (*b*) heat-transfer rate $-\phi'(0)$ with R in the region of largely downflow. The ● correspond to solutions illustrated in figure 8. Arrows indicate increasing $\phi'(0)$ or $f(\infty)$.

$R = 0{\cdot}32414$ ($-\phi'(0) = 0{\cdot}72900$) and $Pr = 11{\cdot}6$ reverses from negative to positive at $\eta = 0{\cdot}015 \pm 0{\cdot}005$. As we noted in §1, the magnitude of these reversals increases significantly as $-\phi'(0)$ decreases towards 0, whereas the magnitudes of the outside reversals remain very small as $f(\infty)$ decreases towards 0.

The behaviour of the temperature profile ϕ is even more dramatic. For $R = 0{\cdot}34920$ and $-\phi'(0) = 0{\cdot}8$, we find that $\phi(4) \approx 0{\cdot}93 \times 10^{-6}$ and $\phi(5) \approx 0{\cdot}3 - 10^{-8}$; while for $R = 0{\cdot}45402$ and $-\phi'(0) = 0{\cdot}005$, we find that $\phi(4) \approx 0{\cdot}95 \times 10^{-1}$ and $\phi(5) \approx 0{\cdot}5 \times 10^{-3}$.

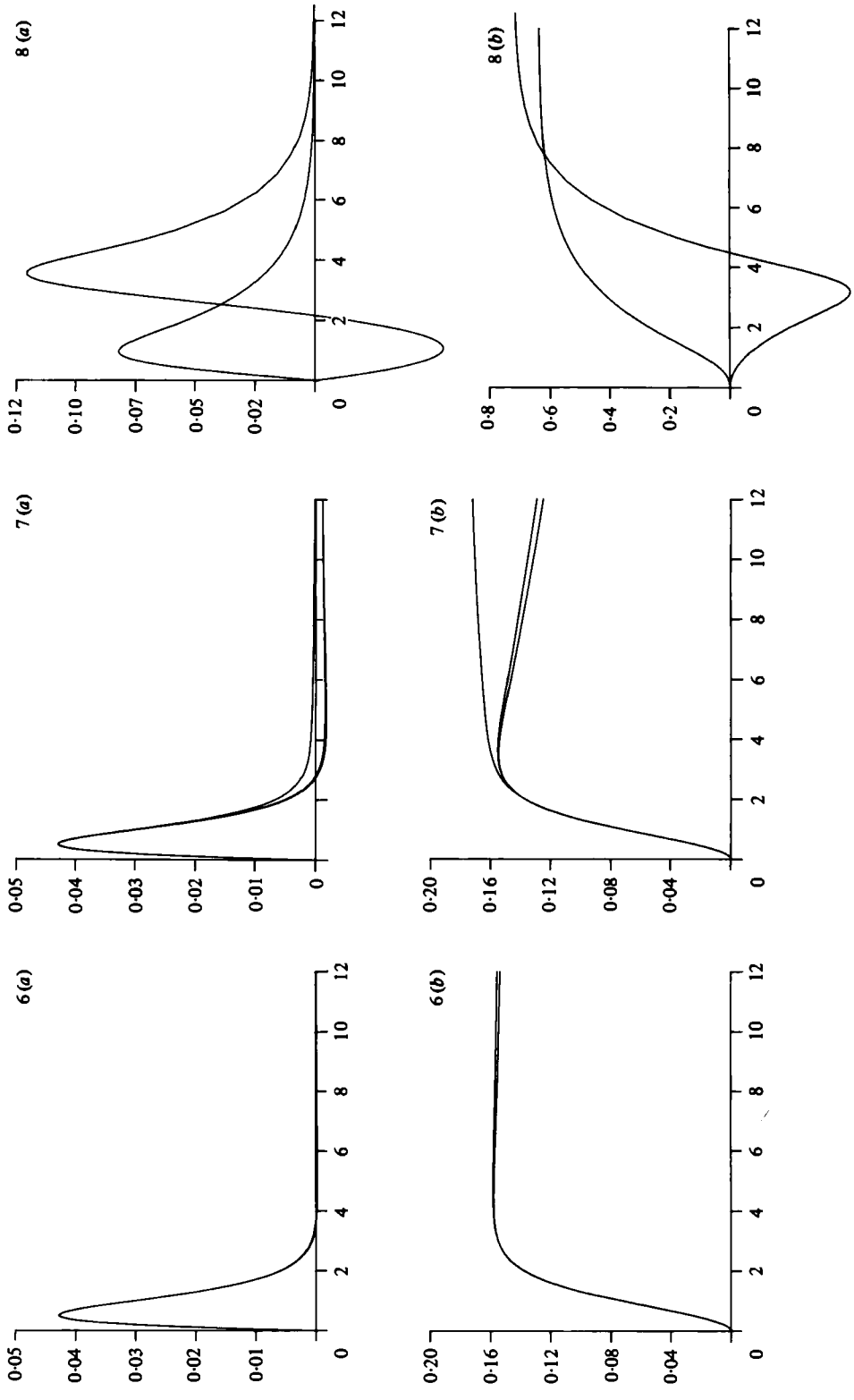
8 (a)
8 (b)
7 (a)
7 (b)
6 (a)
6 (b)
0·12
0·10
0·07
0·05
0·02
0·8
0·6
0·4
0·2
0·20
0·16
0·12
0·08
0·04
0·05
0·04
0·03
0·02
0·01
0
2
4
6
8
10
12

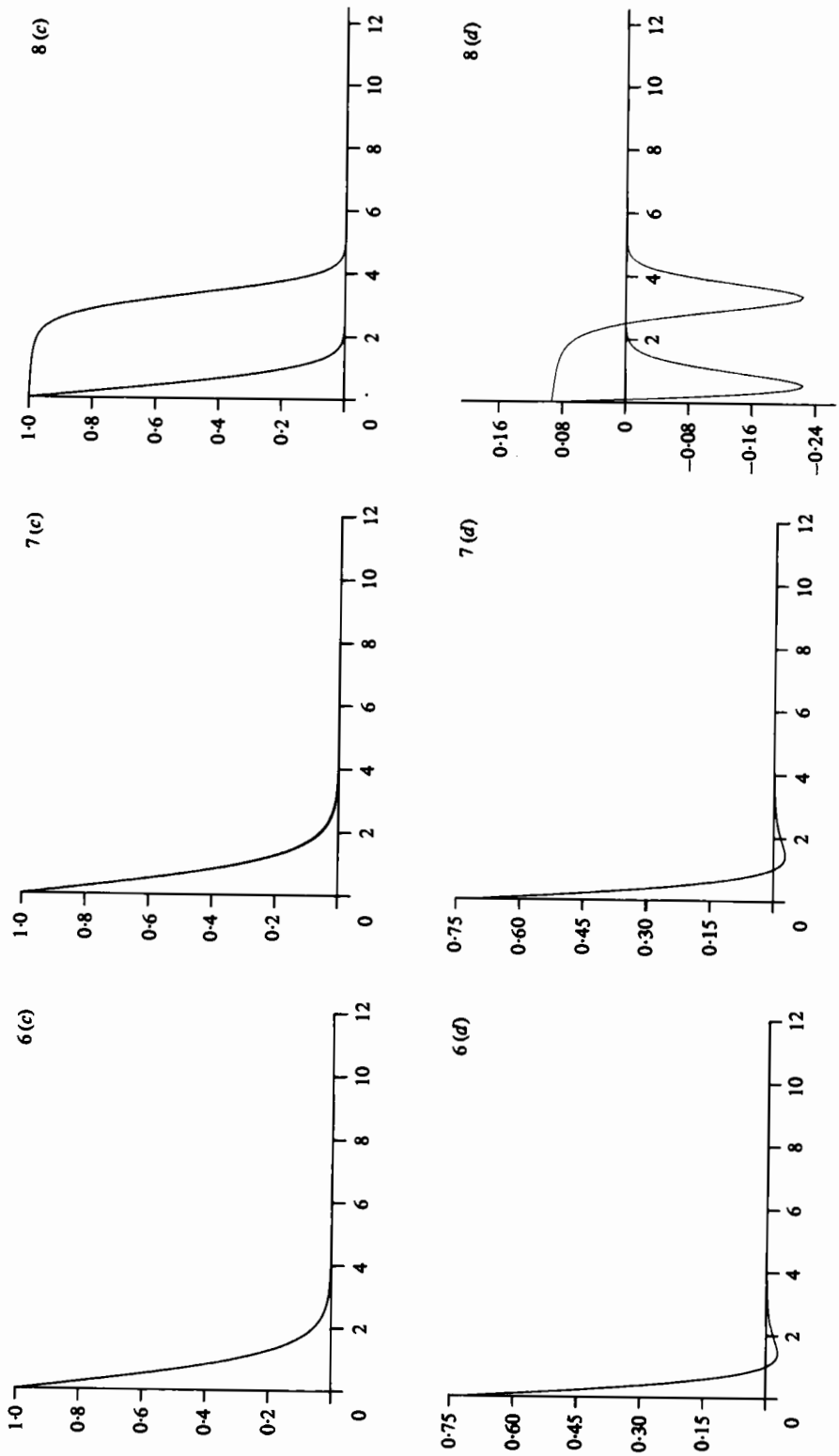

FIGURES 6, 7, 8. (*a*) Tangential velocity component f', (*b*) normal velocity component $3f - \eta f'$, (*c*) temperature-excess ratio ϕ, and (*d*) buoyancy force $W = |\phi - R|^q - |R|^q$, for (6) the two solutions at $R = 0{\cdot}15176$, (7) the three solutions at $R = 0{\cdot}15150$, and (8) the two solutions at $R = 0{\cdot}45402$.

$f(\infty)$	R	$-\phi'(0)$	$f''(0)$	η_∞
0·05900	0·15150	0·80396	0·21303	100
0·05800	0·15155	0·80364	0·21300	100
0·05700	0·15160	0·80334	0·21298	200
0·05600	0·15163	0·80306	0·21296	200
0·05500	0·15166	0·80280	0·21294	200
0·05400	0·15170	0·80254	0·21293	200
0·05300	0·15172	0·80231	0·21292	200
0·05200	0·15174	0·80208	0·21291	200
0·05100	0·15176	0·80187	0·21291	200
0·05000	0·15177	0·80167	0·21291	200
0·04500	0·15180	0·80087	0·21292	200
0·03900	0·15176	0·80025	0·21298	500
0·03000	0·15163	0·79989	0·21309	500
0·01900	0·15150	0·80006	0·21319	500
0·01550	0·15148	0·80020	0·21319	500
0·01500	0·15148	0·80022	0·21319	500
0·01400	0·15148	0·80026	0·21319	500
0·01000	0·15150	0·80043	0·21317	500
0·00500	0·15153	0·80054	0·21314	500

TABLE 1. Solution data at $Pr = 11{\cdot}6$, $q = 1{\cdot}894816$ computed by continuation with respect to $f(\infty)$ in the region of largely upflow

$-\phi'(0)$	R	$f(\infty)$	$f''(0)$	η_∞
0·97520	0·45402	0·21166	+0·13806	100
0·97020	0·45000	0·21098	+0·13453	100
0·54000	0·29296	0·17525	−0·07178	100
0·52000	0·29218	0·17509	−0·07769	200
0·50000	0·29183	0·17507	−0·08334	200
0·49400	0·29181	0·17510	−0·08498	300
0·49250	0·29181	0·17511	−0·08594	300
0·49000	0·29181	0·17512	−0·08607	300
0·46000	0·29237	0·17551	−0·09388	200
0·42000	0·29452	0·17656	−0·10344	200
0·38000	0·29824	0·17822	−0·11202	200
0·34000	0·30351	0·18049	−0·11963	200
0·30000	0·31037	0·18337	−0·12622	300
0·26000	0·31889	0·18686	−0·13174	200
0·22000	0·32919	0·19101	−0·13606	200
0·18000	0·34151	0·19587	−0·13898	200
0·16000	0·34854	0·19860	−0·13982	200
0·14000	0·35625	0·20157	−0·14014	200
0·12000	0·36473	0·20481	−0·13987	200
0·10000	0·37416	0·20838	−0·13885	200
0·08000	0·38476	0·21237	−0·13684	200
0·06000	0·39695	0·21694	−0·13345	200
0·04000	0·41152	0·22241	−0·12784	200
0·03000	0·42024	0·22561	−0·12362	200
0·02000	0·43060	0·22969	−0·11765	200
0·01000	0·44419	0·23507	−0·10804	200
0·00500	0·45402	0·23915	−0·09951	200

TABLE 2. Solution data at $Pr = 11{\cdot}6$, $q = 1{\cdot}894816$ computed by continuation with respect to $\phi'(0)$ in the region of largely downflow

There are some small differences between our computations of solutions and those of Carey *et al.* (1980) for the same solutions. For example, for $R = 0{\cdot}15172$ we find $-\phi'(0) = 0{\cdot}80231$ and $f(\infty) = 0{\cdot}05300$, while Carey *et al.* obtained $-\phi'(0) = 0{\cdot}80232$ and $f(\infty) = 0{\cdot}05305$.

We suspect (but are unable to prove) that as $f(\infty)$ decreases to 0, the curve in figure 4(a) has additional points of vertical tangency akin to those proved rigorously by Hastings & Kazarinoff (1982) for an analogous but simpler system modelling natural convection in saturated porous media. In addition, we expect that as $-\phi'(0)$ decreases to 0, the upper branch of the curve in figure 5(a) and the lower branch of the curve in figure 5(b) tend to limit points. However, these limit points cannot correspond to any solution because there exist no solutions of (2.4)–(2.5) for any R with $\phi'(0) = 0$. The solutions corresponding to points on the lower branch of the curve in figure 5(a) (upper branch in figure 5b) approach the known solutions at increasing values of R.

4. Conclusions and additional observations

These results show the additional complexity that arises in the range $0 < R < 0{\cdot}5$. It is in this range of R that both local buoyancy-force and flow reversals arise. These lead to convective inversion, a reversal from largely upward to largely downward flow. Earliest experiments demonstrated the most evident aspect in this range, convective inversion.

Recent calculations pushed into this R-region from both sides, that is, into conditions of local buoyancy force reversal (Carey *et al.* 1980). They extended to the first local flow reversals, both outside and inside. However, a large gap was left in the middle, for approximately $0{\cdot}15 < R < 0{\cdot}29$, in which solutions could not be obtained by simple shooting methods, even when augmented by use of the asymptotic behaviour of (f, ϕ). Laboratory visualizations showed that very complicated transport arose there. It was often neither steady nor of boundary region form (Carey & Gebhart 1981).

The calculations here have narrowed the width of the gap slightly, to $0{\cdot}15180 < R < 0{\cdot}29181$, for $Pr = 11{\cdot}6$. However, they have also produced an inference that further solutions of the steady-state boundary-layer equations will not be found in the remaining gap. At the least, there are strong indications that there are no direct continuations of the earlier kind of solutions. Finite-difference methods applied to the time-independent form of (2.1) have also failed to find solutions in a similar gap ($0{\cdot}1111 < R < 0{\cdot}2982$) (Wilson & Lee 1981).

However, our new calculations have also shown something of potentially much greater physical significance; that is, multiple steady-state solutions, for single values of R. This occurred over two ranges, each just outside the gap, on each of the lower and the upper sides.

Upon continuing the calculations to less vigorous flows (i.e. flows with smaller $f(\infty) = \int_0^\infty f' d\eta$), to increasing outside flow reversal, and to decreasing R below $0{\cdot}15180$, a second family of solutions arose, to an R-limit of about $0{\cdot}15149$. Then again, continuing to slightly higher values of R, an additional even less vigorous family of flows was found. Thus, three solutions were found for the same value of R over this narrow range. The multiple solutions illustrated in each of figures 6 and 7, at $R = 0{\cdot}15176$ and $R = 0{\cdot}15150$, are quite similar except in the outside flow-reversal region and in

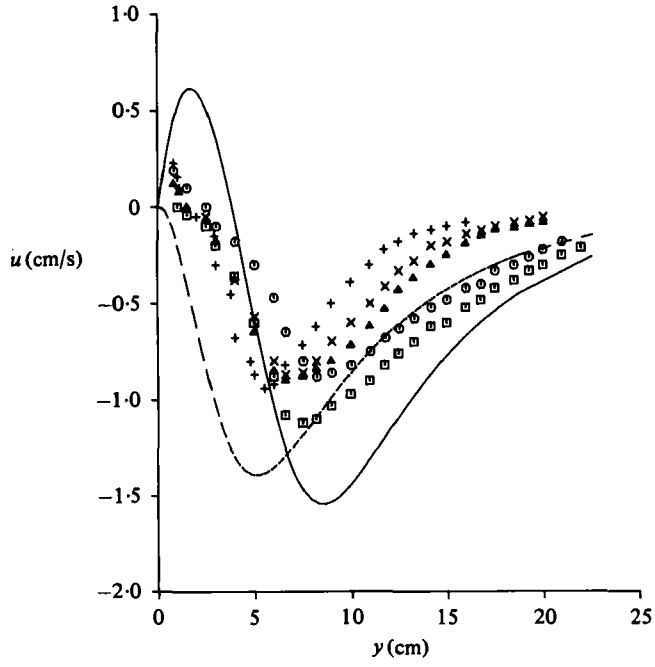

FIGURE 9. Experimental data from Wilson & Vyas (1979) for $R = 0{\cdot}317$ that show unsteady behaviour of the physical vertical velocity component u. Also shown are two curves corresponding to u as calculated from a multiple steady-state solution 'pair' corresponding to $R = 0{\cdot}31889$, $-\phi'(0) = 0{\cdot}26000$ (solid line) and $R = 0{\cdot}31624$, $-\phi'(0) = 0{\cdot}70000$ (dashed line). Symbols, in order of increasing time, are +, ×, ⊡, △, ⊙.

the resulting effect of this on entrainment velocity v. These effects are very different for the solutions at $R = 0{\cdot}15150$ corresponding to $f(\infty) = 0{\cdot}0595$ and $f(\infty) = 0{\cdot}0100$.

Immediately beyond the upper limit point, at $R = 0{\cdot}29181$, the second family of flows were also much less vigorous, with increasing inside flow reversal. Extremely low heat-transfer rates are found at higher values of R. Figure 8 also indicates a tremendous difference in the spatial distribution of vertical momentum. The new flow illustrated in figure 8 is indeed more vigorous than the previously known flow (without inside reversal) illustrated there.

The irreducible gap in the parameter R-range, which remains after these calculations, along with the multiple solutions on each side of the gap, have important implications concerning the question of how increasing buoyancy-force reversals (in from each side of the gap) may trigger convective inversion. The final mechanism may be different, coming from the two sides. Our results of themselves do not provide the mechanisms. They do, however, suggest that any actual flow may be either very unstable, unsteady, or both of these. We have plotted in figures 9 and 10 the vertical velocity profiles of some of the flows we have computed along with some experimental data of Carey & Gebhart (1981) and Wilson & Vyas (1979). These plots are suggestive of the existence of oscillations between unstable steady-state flows. Note that the numerical solutions plotted in figure 10 correspond to R-values far from the R-value corresponding to the data plotted there. These numerical solutions were chosen because they crudely fit the data. The comparison is made only to illustrate that oscillation

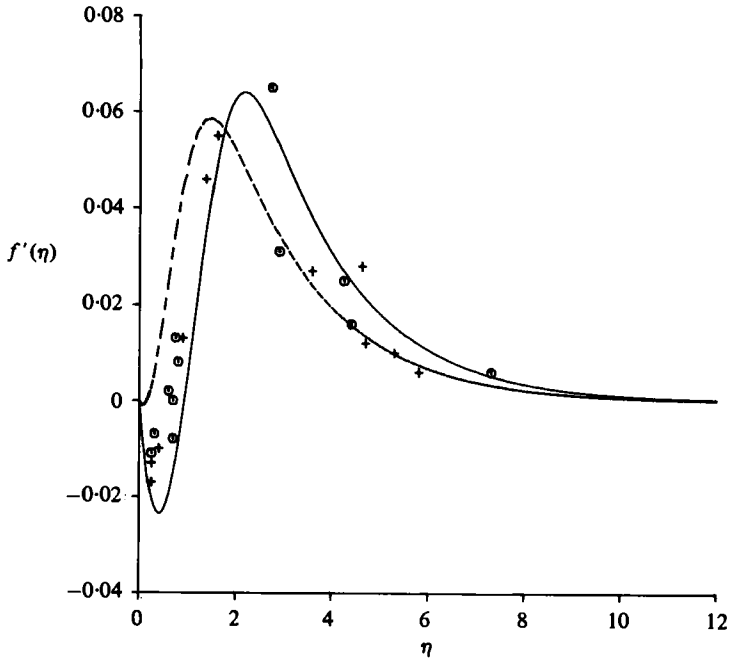

FIGURE 10. Experimental data from Carey & Gebhart (1981) for $R = 0{\cdot}254$ that shows oscillatory behaviour of $f'(\eta)$. The circles and + symbols indicate data taken at two different times. Also shown are two curves corresponding to $f'(\eta)$ results calculated from a multiple steady-state solution 'pair' corresponding to $R = 0{\cdot}30351$, $-\phi'(0) = 0{\cdot}34000$ (solid line) and $R = 0{\cdot}30370$, $-\phi'(0) = 0{\cdot}64000$ (dashed line).

between steady states is one possible explanation for the time fluctuations in the data of Carey & Gebhart (1981). On the other hand, Carey & Gebhart (1981) have observed flows that are in good agreement with theory (see e.g. figures 8 and 9 of their work).

Any tendency of preference between a strong and a weak flow, at any given value of R, would make available relatively large amounts of energy to drive transient effects, to amplify disturbances and/or to reverse the general flow direction. Appreciable differences in flow energy distributions were seen in figure 7, and much larger ones appear in figure 8.

In fact, the measurements cited above indicate that this gap is a region of large time-dependent effects. Measurements also suggest that convective inversion does not always occur at a particular value R_1 of R, that is, of T_∞ for a given value of T_0. No sharp value of R_1 has been found in any largely vertical flow. Different values of R_1 may arise, in the gap, depending on how the bounding conditions are changed to achieve the inversion.

These new results provide a first guide for attempts to interpret the convective motions in this region. The relative hydrodynamic and configurational stability of such flows would be important indicators, as would any determinations of the general characteristics of transient flows.

The authors acknowledge support from the following grants: SUNY RES. FDN.-150-7548-A (I.E. and N.K.), NSF-CME77-21641 (B.G.), NSF-MCS7905790 (B.H.), NSF-MCS8100727 (N.K. and J.M.). The authors thank Bonnie Boskat for her expert efforts in the preparation of the manuscript and Jinn-Yuh Jang for help with the figures.

REFERENCES

ASCHER, U., CHRISTIANSEN, J. & RUSSELL, R. D. 1978 COLSYS – a collocation code for boundary-value problems. *Codes for Boundary-Value Problems in Ordinary Differential Equations* (ed. G. Goos & J. Hartmanis). Lecture Notes in Computer Science, vol. 76, pp. 164–185. Springer.

BENDELL, M. S. & GEBHART, B. 1976 Heat transfer and ice melting in ambient water near its density extremum. *Int. J. Heat Mass Transfer* **19**, 1081–1087.

BULIRSCH, R. & STOER, J. 1966 Numerical treatment of ordinary differential equations by extrapolation methods. *Numer. Math.* **8**, 1–13.

BULIRSCH, R., STOER, J. & DEUFLHARD, P. 1982 Numerical solution of nonlinear two-point boundary values problems. *Numer. Math., Handbuch Series*, to appear.

CAREY, V. P. & GEBHART, B. 1981 Visualization of the flow adjacent to a vertical ice surface melting in cold pure water. *J. Fluid Mech.* **107**, 37–55.

CAREY, V. P., GEBHART, B. & MOLLENDORF, J. C. 1980 Buoyancy force reversals in vertical convection flows in water. *J. Fluid Mech.* **97**, 279–297.

COHEN, D. S. 1973 Multiple solutions of nonlinear partial differential equations. In *Nonlinear Problems in the Physical Sciences and Biology* (ed. I. Stakgold, D. D. Joseph & D. H. Sattinger). Springer.

DIEKHOFF, H.-J., LARY, P., OBERLE, H. J., PESCH, H.-J., RENTROP, P. & SEYDEL, R. 1977 Comparing routines for the numerical solution of initial value problems of ordinary differential equations in multiple shooting. *Numer. Math.* **27**, 449–469.

GEBHART, B., CAREY, V. P. & MOLLENDORF, J. C. 1979 Buoyancy induced flows due to energy sources in cold quiescent pure and saline water. *Chem. Engng Trans.* **3**, 555–575.

GEBHART, B. & MOLLENDORF, J. C. 1977 A new density relation for pure and saline water. *Deep Sea Res.* **24**, 813–848.

GEBHART, B. & MOLLENDORF, J. C. 1978 Buoyancy-induced flows in water under conditions in which density extremes may arise. *J. Fluid Mech.* **89**, 673–707.

HASTINGS, S. P. & KAZARINOFF, N. D. 1982 Multiple solutions for a problem in buoyancy-induced flow. *Preprint.*

JOHNSON, R. S. 1979 Transport from vertical pure water ice surface melting in saline water. Masters thesis, SUNYAB.

LEES, L. & REEVES, B. L. 1964 Supersonic separated and reattaching laminar flows: I. General theory and application to adiabatic boundary-layer/shock-wave interactions. *A.I.A.A. J.* **2**, 1907–1920.

LENTINI, M. & KELLER, H. B. 1978 Computation of Karman swirling flows. In *Codes for Boundary-Value Problems in Ordinary Differential Equations* (ed. G. Goos & J. Hartmanis). Lectures Notes in Computer Science, vol. 76, pp. 89–100. Springer.

LENTINI, M. & KELLER, H. B. 1980 The von Karman swirling flows. *SIAM J. Appl. Math.* **38**, 52–64.

MOLLENDORF, J. C., JOHNSON, R. S. & GEBHART, B. 1981 Several plume flows in pure and saline water at its density maximum. *J. Fluid Mech.* **113**, 269–282.

ORIMI, P. & REEVES, B. L. 1976 Analysis of leading-edge separation-bubbles on airfoils. *A.I.A.A. J.* **14**, 1549–1555.

STEWARTSON, K. 1953 Further solutions of the Falkner–Skan equation. *Proc. Camb. Phil. Soc.* **50**, 454–465.

WILSON, N. W. & LEE, J. J. 1981 Melting of a vertical ice wall by free convection into fresh water. *Trans. A.S.M.E.* C, *J. Heat Transfer* **103**, 13–17.

WILSON, N. W. & VYAS, B. D. 1979 Velocity profiles near a vertical ice surface melting into fresh water. *Trans. A.S.M.E.* C, *J. Heat Transfer* **10**, 313–317.

ZANDBERGEN, P. J. & DIJKSTRA, D. 1977 Non-unique solutions of the Navier–Stokes equations for the Karman swirling flow. *J. Engng Math.* **11**, 167–188.